

Effects of close binary evolution on the main-sequence morphology of young star clusters

CHEN WANG,¹ NORBERT LANGER,¹ ABEL SCHOOTEMEIJER,¹ NORBERTO CASTRO,² SYLVIA ADSCHIED,¹ PABLO MARCHANT,³
AND BEN HASTINGS¹

¹*Argelander-Institut für Astronomie, Universität Bonn, Auf dem Hügel 71, 53121 Bonn, Germany*

²*AIP Potsdam, An der Sternwarte 16, 14482 Potsdam, Germany*

³*Department of Physics and Astronomy, Northwestern University, 2145 Sheridan Road, Evanston, IL 60208, USA*

(Received 2019 November 18; Revised 2019 December 10; Accepted 2019 December 11)

Submitted to ApJL

ABSTRACT

Star clusters are the building blocks of galaxies. They are composed of stars of nearly equal age and chemical composition, allowing us to use them as chronometers and as testbeds for gauging stellar evolution. It has become clear recently that massive stars are formed preferentially in close binaries, in which mass transfer will drastically change the evolution of the stars. This is expected to leave a significant imprint in the distribution of cluster stars in the Hertzsprung–Russell diagram. Our results, based on a dense model grid of more than 50,000 detailed binary-evolution calculations, indeed show several distinct, coeval main-sequence (MS) components, most notably an extended MS turnoff region, and a group of near-critical rotating stars that is spread over a large luminosity range on the red side of the classical MS. We comprehensively demonstrate the time evolution of the features in an animation, and we derive analytic expressions to describe these features. We find quantitative agreement with results based on recent photometric and spectroscopic observations. We conclude that while other factors may also be at play, binary evolution has a major impact on the MS morphology of young star clusters.

Keywords: stars: massive – stars: rotation – stars: evolution – binaries: general

1. INTRODUCTION

The stellar main sequence (MS) in the Hertzsprung–Russell (HR) diagram, which was discovered (Russell 1914) before it was known that stars are powered by nuclear fusion (Atkinson & Houtermans 1929), is the backbone of our knowledge of stars. Until today, the analysis of star clusters has given essential clues for understanding the internal structure and evolution of stars. Research in recent years has shown that the MSs of star clusters are not simple one-dimensional structures; rather, they contain distinct features that still need to be deciphered.

In studies of star clusters, frequent key assumptions are that the stars in a cluster are coeval, have the same initial chemical composition, are not affected by rotation, and are single stars. All four assumptions are currently being challenged by modern, high-precision observations. Recently, photometric studies using the Hubble Space Telescope revealed that the MS of young and intermediate age star clusters (14–600 Myr) in the Magellanic Clouds and in the Galaxy is split into two distinct MSs, as well as an extended MS turnoff region (D’Antona et al. 2017; Milone et al. 2018; Li et al. 2019, and references therein). Furthermore, the young clusters show distinct groups of emission-line stars, extending more than two magnitudes below the turnoff (Milone et al. 2018), most of which are spectroscopically identified as Be stars (Bodensteiner et al. 2019).

In this situation, it appears worthwhile to investigate binary-evolution effects. The observed binary incidence and binary properties of massive stars imply that an isolated life of a massive star is the exception, the rule being that its

evolution will be strongly affected by a binary companion (Sana et al. 2012). Simplified binary population synthesis calculations in which binary evolution is approximated based on single-star models, have shown that binary evolution can produce a rapidly rotating sub-population (de Mink et al. 2013), and that it can account for the so-called blue stragglers, i.e., cluster stars above the apparent cluster turnoff, in Galactic open clusters with ages of up to ~ 1 Gyr (Yang et al. 2011; Schneider et al. 2015). However, such so called rapid binary-evolution models are not able to predict reliable effective temperatures of post-interaction stars. To understand the MS morphology of young star clusters, it is therefore necessary to investigate the effects of close binary evolution based on dense grids of detailed binary-evolution models (van Bever & Vanbeveren 1998).

Here, we provide such grids, which include differential rotation, rotationally induced internal mixing, and magnetic angular momentum transport as used by Marchant et al. (2017) and use them to investigate the effects of close binary evolution on the MS morphology of young star clusters. In Sect. 2 we describe the adopted physics to compute binary models, and we present our main results in Sect. 3. We provide a comparison with single-star models in Sect. 4, and with observed star clusters in Sect. 5. In Sect. 6, we give our concluding remarks.

2. METHOD AND ASSUMPTIONS

We use the detailed one-dimensional stellar evolution code MESA (Paxton et al. 2011, 2013, 2015), version 8845, to compute our binary-evolution models. The stellar models contain physics assumptions that are identical to the rotating single-star models of Brott et al. (2011), and include differential rotation, rotationally induced internal mixing, magnetic angular momentum transport, stellar wind mass loss, and non-equilibrium CNO nucleosynthesis. Our assumptions on binary physics are as those described by Marchant et al. (2017). Below, we emphasize the most relevant physical assumptions for convenience.

We use the standard mixing-length theory to model convection with a mixing-length parameter of $\alpha = l/H_P = 1.5$, where H_P denotes the local pressure scale height, which allows for inflated envelopes in models near their Eddington limit (Sanyal et al. 2015, 2017). To determine the boundaries of convective zones, we adopt the Ledoux criterion, where we include convective core overshooting as a step function with $\alpha_{\text{OV}} = 0.335$ (Brott et al. 2011). We include semiconvective mixing in superadiabatic layers if they are stable according to the Ledoux criterion using $\alpha_{\text{sc}} = 1$ (Langer et al. 1983), and thermohaline mixing as used by Cantiello & Langer (2010) with $\alpha_{\text{th}} = 1$. Rotationally induced mixing is modeled as a diffusive process (Heger et al. 2000). We take into account the effects of dynamical and secular shear instabilities, the Goldreich-Schubert-Fricke instability, and Eddington-Sweet circulations. The efficiency parameter of rotational mixing is $f_c = 1/30$ as proposed by Chaboyer & Zahn (1992). We also include the Tayler-Spruit dynamo for the transport of angular momentum (Spruit 2002; Heger et al. 2005).

The detailed structure of both binary components is computed simultaneously with the orbital evolution. We assume circular orbits and adopt initial spins such that the rotation period of both stars is synchronized to the orbital period of the binary on the zero-age MS. During the evolution, the effects of tidally induced spin-orbit coupling (Detmers et al. 2008) are included. We compute mass and angular momentum transfer arising from Roche-lobe overflow. We assume the specific angular momentum accreted by the secondary star depends on whether the accretion is ballistic or occurs via a Keplerian disk, and restrict the mass accretion of the mass gainer when it has reached near-critical rotation (Petrovic et al. 2005). We do so by adopting a rotational enhancement of the stellar mass-loss rate, which prevents models from exceeding critical rotation (Langer 1998, 2012; Paxton et al. 2015). When the energy contained in the combined luminosity of both stars is insufficient to drive the mass out of the binary at a rate equal to the mass loss rate, we assume that both stars are engulfed in the excess material, with a binary merger ensuing.

For contact phases, we employ the scheme described by Marchant et al. (2016) to model the mass-transfer phase. We assume both stars to merge when they both fill their Roche volumes and mass outflow through the second Lagrangian point is obtained. When a binary merger is assumed to happen for a given binary model while both stars still burn hydrogen in their cores, we calculate its further evolution by adopting a single-star model with the appropriate mass and age. We assume that the internal structure fully rejuvenates, and adopt an initial central hydrogen abundance of the merger product according to Schneider et al. (2016). Mergers are treated as non-rotating stars, following Schneider et al. (2019).

The evolution of the binary models is started by considering both stars on the zero-age MS. We then follow the evolution of both components, as long as one of the two stars is still on the MS. We compute our models until core carbon exhaustion. If at that stage the core of a model exceeds the Chandrasekhar mass, we assume that it produces a supernova explosion, and compute the continued evolution of its core hydrogen burning companion in isolation.

We adopt a metallicity of $Z_{\text{SMC}} = 0.002179$ appropriate for young stars in the SMC, a helium abundance of $Y = 0.25184$, and a distribution of heavy elements as used by [Brott et al. \(2011\)](#). Our model grid covers initial primary star masses between $5 M_{\odot}$ and $100 M_{\odot}$, initial mass ratios of 0.95-0.3, and initial orbital periods of 1 day-8.6 yr. We cover the initial parameter space with more than 50,000 binary-evolution models, using 26 different initial primary masses and 140 initial period values, both distributed evenly in log-space, and 14 evenly distributed initial mass ratios.

We compute a second suite of binary models in order to predict the distribution of stars in the HR diagram of a star cluster with a total mass of $10^5 M_{\odot}$ in stars between $100 M_{\odot}$ and $0.8 M_{\odot}$. This leads to 2078 binary systems with primary masses larger than $5 M_{\odot}$. We use a Monte Carlo simulation to generate initial binary systems adopting a Salpeter initial mass function (IMF) ([Salpeter 1955](#)), a flat distribution of initial mass ratios q_i , and a flat distribution of $\log P_i$, within the initial mass ratio and period ranges as described above. We assume a binary fraction of one, i.e., we do not consider additional single stars in our cluster model. We use the MESA code to evolve the generated 2078 binary systems in time. In this way, the time dependence of the HRD distribution of the cluster stars can be simulated without the need to interpolate between different binary-evolution models. An interpolation in time is still necessary, which, due to the high time resolution of the MESA models, does not lead to noticeable errors.

3. BINARY-INDUCED MAIN-SEQUENCE FEATURES

[Figure 1](#) shows the locations of our models in the HR diagram for selected ages. Each of the $\sim 50,000$ detailed binary evolutionary sequences provides one dot in each figure, as long as at least one of the two stars still undergoes core hydrogen burning. We only plot the visually brighter component of each system, as in most cases the fainter one is either unevolved, lost its envelope, or terminated its evolution ([de Mink et al. 2014](#)). Statistical probabilities due to the IMF or initial binary parameter distributions are not taken into account, but the figure is meant to demonstrate which parts of the HR diagram are covered by models in the different evolutionary branches. In this figure, we distinguish models in four different evolutionary branches, as indicated.

The pre-interaction binaries (blue) in [Fig. 1](#) are located on a single line, which represents the corresponding single-star isochrone (SSI). As most of our pre-interaction stars rotate slowly by construction, the rotational broadening of the SSI is small, even near the turnoff (see [Figure 7](#) of [Brott et al. 2011](#)). This ensures that all other features that are visible in [Fig. 1](#) are induced by binary evolution, and not an effect of the initial distribution of rotational velocities.

We distinguish three prominent features in the distribution of stars in [Fig. 1](#). First, at all times, the turnoff region is extended beyond the SSI, mostly to higher luminosities and temperatures (we call this the turnoff binary-evolution feature, TBF). Second, for ages above ~ 4 Myr, a distinct red MS appears (red binary-evolution feature, RBF), whose lower part is well separated from the SSI. Third, at all times, MS stars to the blue side of the SSI appear. They form a separated blue MS for ages above ~ 10 Myr and merge with the TBF at high luminosities (blue binary-evolution feature, BBF). We indicate these features in [Panel \(d\)](#) of [Fig. 1](#). None of these three features has been described by detailed binary-evolution models before.

The evolution of exemplary binary models in the HR diagram in [Fig. 2](#) helps reveal the origin of the MS features. Binaries that undergo mass transfer while both stars fuse hydrogen in their cores (Case A mass transfer) evolve into semi-detached systems. This occurs because Case A mass transfer comprises a nuclear timescale mass-transfer phase, whereas otherwise mass transfer occurs on the much shorter thermal or even on the dynamical timescale. As shown in [Fig. 1](#), the semi-detached models do not give rise to a sharp feature in the HR diagram, since their locations are quite spread out, and overlap strongly with those of the mergers and post-mass-transfer systems. These together produce the TBF. They are mostly located above and to the left of the line formed by the pre-interaction stars because their mass ratios are inverted, since the former secondary stars have accreted substantial amounts of matter in a preceding thermal timescale Case A mass transfer. If the secondary's mass has been increased to values above the mass corresponding to the single-star turnoff, it will be brighter than any of the pre-interaction stars at the given age. The internal process of rejuvenation, i.e., the mixing of fresh fuel toward the centre due to an increase of the mass of the convective core, makes it look younger, i.e., leads to a higher surface temperature than that of a comparable pre-interaction star ([Schneider et al. 2015](#)). After the mass donor in a Case A binary system ends its core hydrogen burning, its post-MS expansion will give rise to another rapid, thermal timescale, mass-transfer phase, after which we consider the binary a post-mass-transfer system.

Our Case A binaries produce a rich spectrum of observable features. The BBF, as described above, is exclusively due to Case A mass transfer. Whereas models in the extended turnoff region are blue mainly because they are rejuvenated,

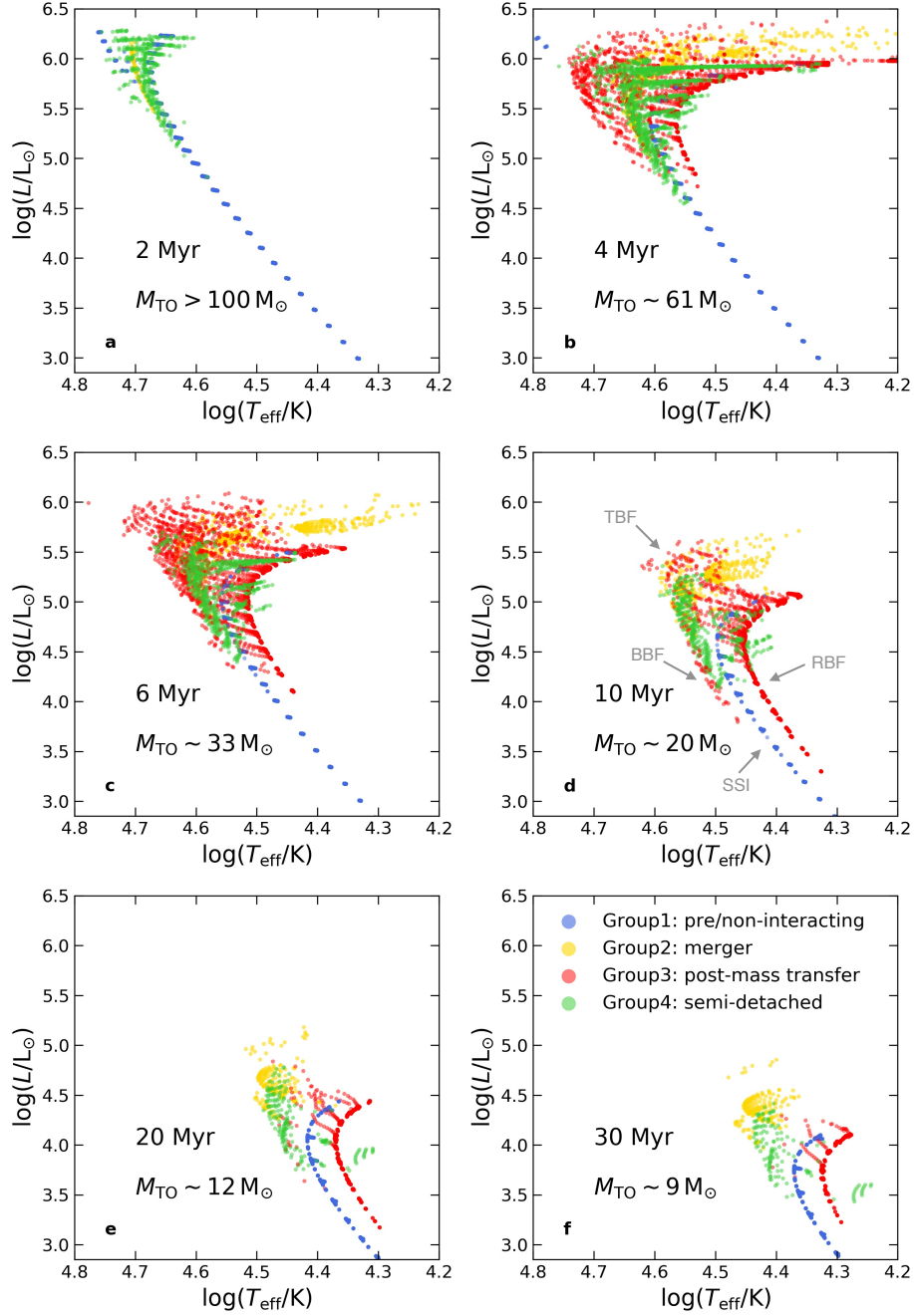


Figure 1. Distribution of our binary models in the Hertzsprung-Russell diagram at six different times, as indicated. Only the visually brighter component of each binary is plotted, for all models where at least one of the two stars still undergoes core hydrogen burning. Dark blue dots correspond to models that have not yet interacted with a companion. Yellow dots indicate the products of the merger of two core hydrogen burning stars. Red dots indicate stars that have undergone rapid (thermal timescale) accretion of matter from a companion. Green dots represent stars undergoing nuclear timescale accretion at the selected time. Below the age, we indicate the approximate MS turnoff mass for the non-interacting stars. We indicate the binary produced MS features in Panel (d).

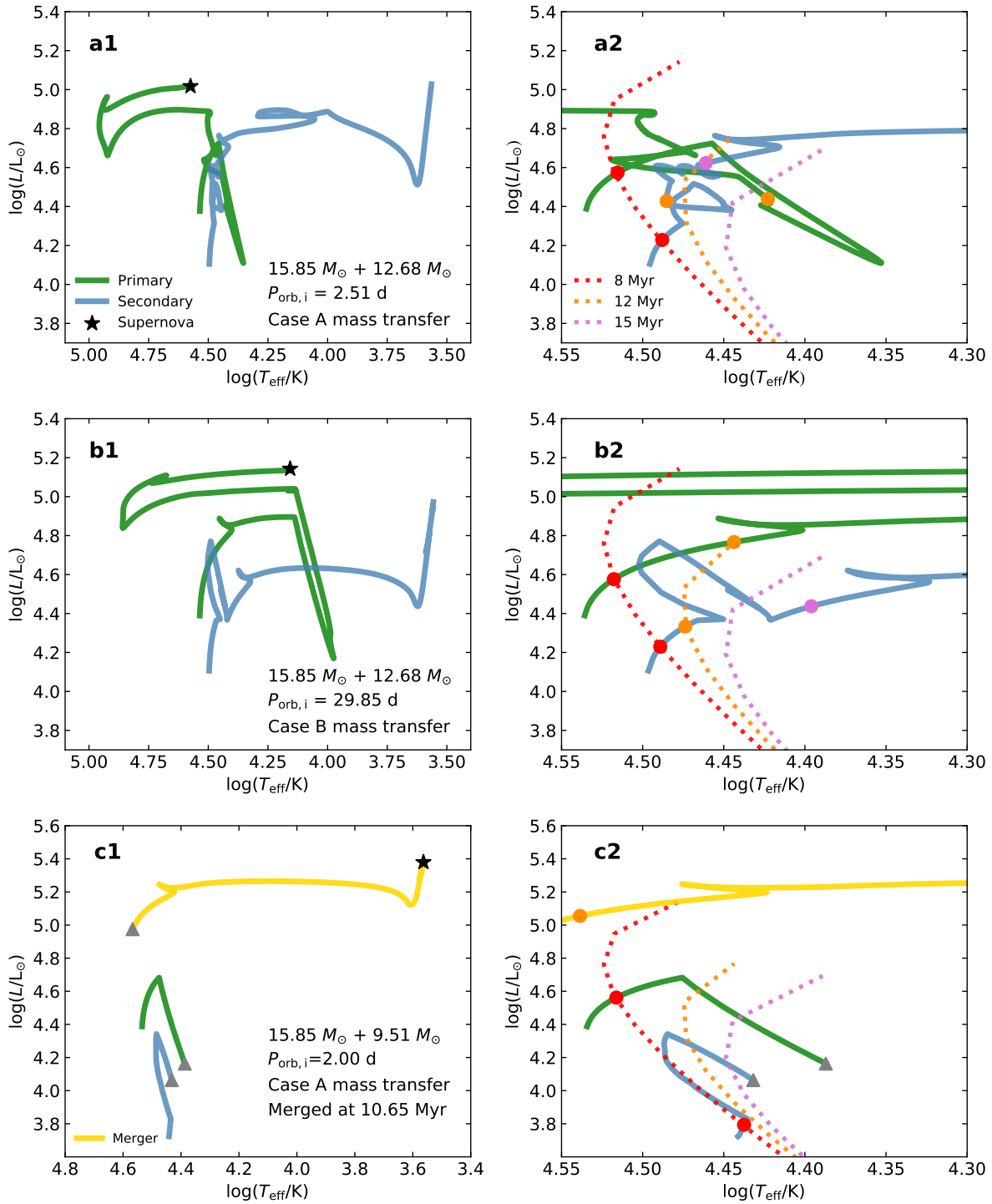


Figure 2. Evolution of both components of three example binary models in the HR diagram (left panels), with a zoom of the MS region (right panels). All three models start with the same primary model (donor star, green lines) of $15.85 M_{\odot}$. The initial mass of the secondary stars (mass gainer, blue lines) is $12.68 M_{\odot}$ in the top two systems, and $9.51 M_{\odot}$ in the third. The dashed lines in the right panels represent single-star isochrones for 8, 12, and 15 Myr, and solid dots on the evolutionary tracks with the corresponding colors mark the positions of the binary components at these ages. The black star symbols mark the pre-supernova position of the primary stars. The gray triangles in the bottom panels mark the merger event. The donor stars in the top and the bottom models start mass transfer during core hydrogen burning (Case A mass transfer), and the donor in the middle model starts mass transfer after core hydrogen exhaustion (Case B mass transfer).

the fainter blue MS stars of the BBF, which are most pronounced for ages in the range of 10-20 Myr, have higher surface temperatures because their envelopes are significantly enriched in helium. They originate from the binaries with the shortest initial periods and smallest initial mass ratios, which undergo contact evolution but avoid merging (Marchant et al. 2016). Furthermore, we find some detached systems in between fast and slow Case A mass transfer, which share their HR diagram positions with the semi-detached systems. At the highest masses, strong stellar winds can lead to a widening of the orbit after the fast Case A mass transfer. This may detach the mass donor from its Roche lobe for some time (Petrovic et al. 2005). At lower masses, the orbital period of systems right after the fast Case A mass transfer can be short enough that tidally induced spin-orbit coupling leads to an expansion of the orbit, which again allows the primary stars to detach from their Roche lobe for about 0.1-0.2 Myr before the slow Case A mass transfer begins. We also find some semi-detached binary models in which the mass donor is still the brighter of the two stars. These donor stars, which are in thermal equilibrium, can be significantly cooler than the single-star terminal age MS. In Fig. 1, we see these models sticking out on the cool side of the RBF about 0.5 dex below the turnoff. We note that such systems have been identified by Howarth et al. (2015) and Mahy et al. (2019). Finally, our merged stars behave similar to near-conservative Case A mass-transfer systems. They populate the brightest part of the extended turnoff region and overlap strongly with the post-mass-transfer mass gainers (Fig. 1).

The group of post-mass-transfer systems is dominated by initially wider binaries, which undergo thermal timescale mass transfer only after the primary star exhausted hydrogen in its core (Case B mass transfer). As their large orbital separations render tides ineffective on the mass gainers, these are quickly spun up to near-critical rotation, after which their accretion efficiencies are strongly reduced (see Section 2). Many Case B mass gainers end up naturally in this situation, as critical rotation is reached after only accreting a few percent of their initial mass (Packet 1981), if the orbits are wide enough to avoid tidal spin-down (Langer 2012). These models populate the RBF, and are approximately 15% cooler than the correspondingly luminous models on the SSI due to the action of their centrifugal force on their structure (Paxton et al. 2019). The RBF becomes more distinct and spreads over a larger luminosity range for larger ages. The RBF shows a temperature offset from the SSI of approximately 15%. Our models are spun up to as fast a rotation as is numerically allowed, i.e., 98% of critical rotation, and they mostly remain at this level for their remaining hydrogen burning lifetimes. Only the most massive fast rotators ($M \gtrsim 20 M_{\odot}$) have strong enough stellar winds to spin down (Langer 1998). This leads them to slowly evolve off the RBF towards the blue side. The RBF extends a factor of 30 or more in luminosity below the turnoff region. We show in Appendix A.2 that the minimum luminosity of the RBF is set by the minimum initial mass ratio for which a merging of the two stars is avoided.

We provide an animation of our population synthesis study (Fig. 3) to demonstrate the time evolution of the various binary-induced morphological MS features of young star cluster. In this animation, different colors correspond to different fractions of critical rotation. A slow forwarding of the image sequence therefore allows tracing of the evolution of the brighter stars in the HR diagram, as well as the evolution of their rotation velocities.

4. COMPARISON TO SINGLE-STAR MODELS

Figure 4 shows the result of a population synthesis for single-star models (Brott et al. 2011) with an age of 15 Myr, for which we adopted the initial rotational velocity distribution of Dufton et al. (2013) and the Salpeter IMF. It demonstrates that rapidly rotating single-star models are significantly bluer than the spun-up mass gainers. Since the rotation rate of the RBF models was ordinary before accretion, they have established a strong chemical gradient in their interior, which prevents rotational mixing from affecting their chemical structure. The situation is different in rapidly rotating single stars, where helium mixed into the stellar envelopes (Brott et al. 2011; Georgy et al. 2013) can cause the star to evolve to a higher effective temperature (Maeder 1987). Furthermore, rapidly rotating stars would only form a discrete MS line if their initial rotation rates were nearly identical, since the amount of mixing is a sensitive function of the rotation rate.

Figure 4 shows also that rotational mixing in single stars can produce an extended turnoff region similar to the TBF. However, the presence of the single-star feature depends on the number of stars that rotate very rapidly initially. If the rapidly rotating single stars were in fact binary products, as suggested by de Mink et al. (2013) and Ramírez-Agudelo et al. (2015), binaries would be the only way to produce an extended MS turnoff. As shown by our models, a TBF is in fact unavoidable for a non-vanishing binary fraction.

5. COMPARISON TO OBSERVED STAR CLUSTERS

Within the last decade or so, it has become evident that extended MS turnoffs are a ubiquitous feature of young star clusters (Li et al. 2019, and references therein). In a broader sense, this includes the phenomenon of the blue

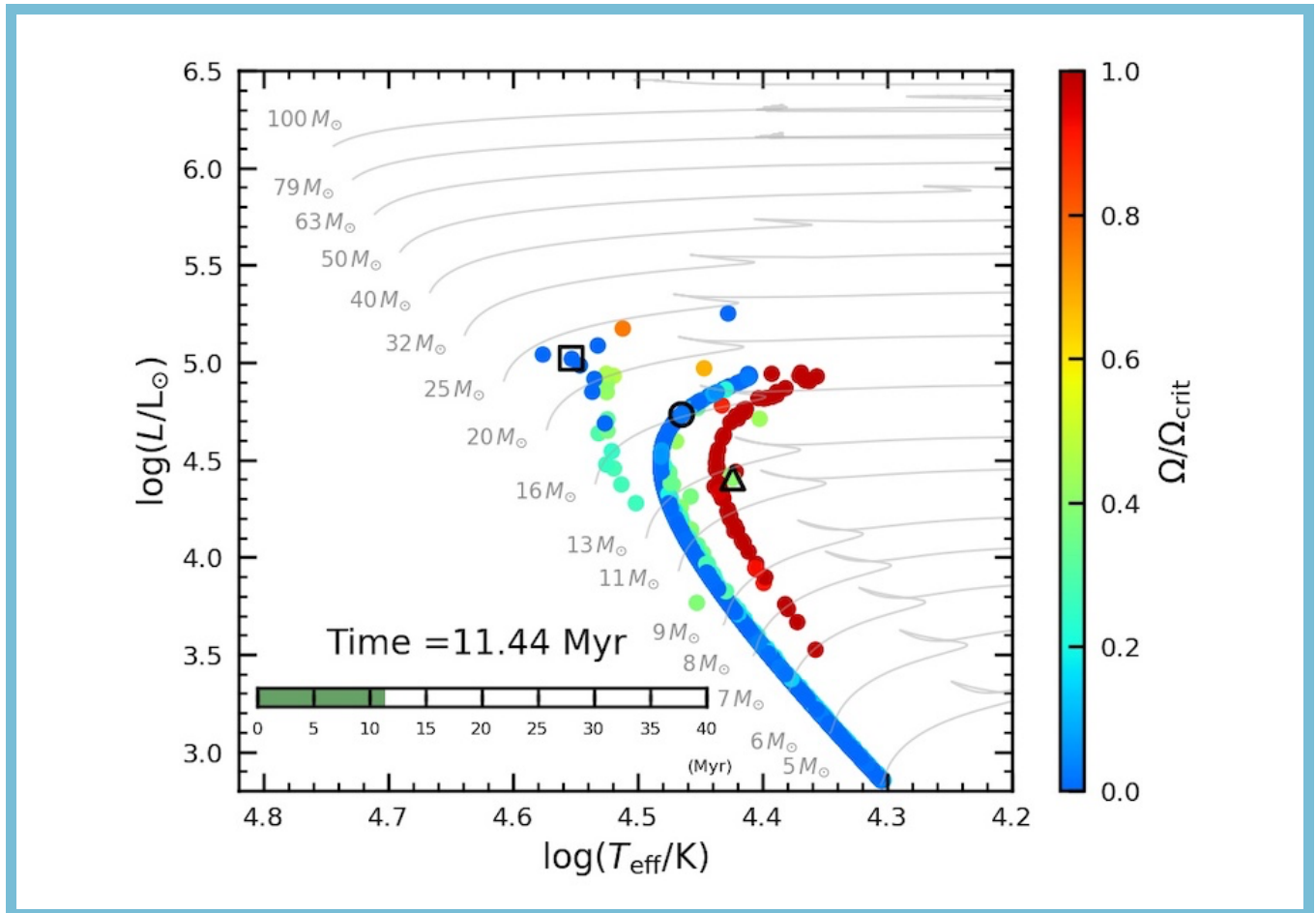


Figure 3. Star cluster animation to show their evolution in the Hertzsprung-Russell diagram, with colors indicating the ratio of rotation to critical rotation velocity. Evolutionary tracks of non-rotating single stars are shown as gray lines, with initial masses quoted. We evolve our cluster from an age of 0.02 Myr up to 40 Myr, corresponding to a turnoff mass of $\sim 8 M_{\odot}$. The three example binaries shown in Fig. 2 are marked with special symbols, such that triangles, circles and squares indicate examples a, b, and c, respectively. The video duration is 20 s. The animation can be downloaded from the link for ancillary files or on the online journal <https://doi.org/10.3847/2041-8213/ab6171>.

stragglers, which is found for clusters of all ages (Ahumada & Lapasset 2007). For young clusters, extended turnoffs are often explained by the presence of stars with a wide range of rotation rates (D’Antona et al. 2017, and references therein). However, simplified binary-evolution population synthesis demonstrates that binary evolution may also be able to lead to extended turnoffs (Yang et al. 2011; Schneider et al. 2014).

Our binary-evolution models allow us to obtain a reliable quantification of the extent of the TBF. We derived the apparent age difference Δt between the SSI and an SSI that fits either the bluest or the brightest member of the coeval binary population in our simulated cluster (see Fig. 3), as a function of its true age t . Figure 5 shows that the apparent age difference can be approximated by a linear function, i.e., $\Delta t \propto t/2$. This corresponds well to our analytic estimate in Appendix A.1 of $\Delta t \propto 0.58t$. As shown in Fig. 5, our result is compatible with the recent observational estimates by Beasor et al. (2019) and Britavskiy et al. (2019). Our analytic result also agrees with corresponding estimates for clusters up to 1000 Myr (see Figure 2 of Niederhofer et al. 2015).

In fact, any process that enriches the core with a fixed fraction of the hydrogen mass of the envelope of a MS star will give rise to a linear relation between the apparent age difference at the turnoff and the turnoff age of the non-enriched stars, be it binary rejuvenation as in our case, or rotationally induced mixing (Niederhofer et al. 2015). However, our simple result, i.e., that the apparent cluster age is about half the true age, is a natural consequence that binary evolution can lead to stars with a mass of about twice the single-star turnoff mass. While rotational mixing can lead to a similar result, a tuning of the rotation rate and/or of the mixing efficiency is required, since the amount of

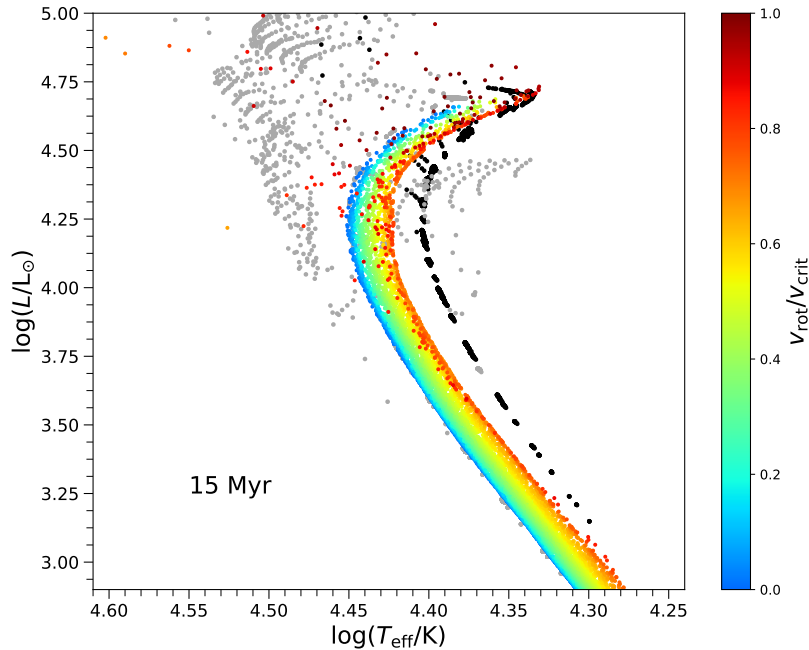


Figure 4. Distribution of 10,000 simulated single stellar models (colored dots) obtained from interpolating in the dense grid of the single-star evolution model of [Brott et al. \(2011\)](#), taking into account the initial mass function and the distribution of the initial rotation velocities derived by [Dufton et al. \(2013\)](#), at 15 Myr. The color represents the ratio of rotation to critical rotation velocity at an age of 15 Myr, according to the color bar to the right. Overlaid are our binary-evolution models using grey and black dots, at the same age, with black indicating a ratio of rotation to critical rotation velocity above 0.98.

mixed material depends on both parameters. In any case, it appears likely that binary evolution provides a significant, perhaps dominant, contribution to the extended turnoffs in young star clusters.

The occurrence of the RBF in our models is a genuine binary-evolution effect and does not depend on the choice of initial rotation rates. The effectiveness of accretion-induced spin-up in nature is demonstrated by the observed group of Be/X-ray binaries, which are understood as rapidly rotating B stars that have accreted from the progenitors of neutron star companions ([Wang et al. 2018](#)). We therefore identify our RBF models, which all rotate extremely rapidly (see Fig. 3), as Be stars ([Pols et al. 1991](#)). Recent photometric and spectroscopic results show that a significant fraction of the MS stars in young clusters ($\lesssim 100$ Myr) within two to three magnitudes below the turnoff are Be stars ([Milone et al. 2018](#); [Bodensteiner et al. 2019](#)). As demonstrated by our animation (Fig. 3), noting that a difference of 2.5 mag corresponds to a factor of 10 in luminosity, this brightness range is well reproduced by our binary models. In Sect. A.2 we relate this range analytically to the minimum mass ratio of stable Case B mass transfer, which thus can be directly determined from the quoted observations.

It has been shown by [Ekström et al. \(2008\)](#) that if stellar winds are not too strong, rotating single stars increase their fraction of critical rotation during the MS evolution, which may lead the initially fastest rotators to become Be stars. However, the transition to the Be stage occurs mostly at the end of core hydrogen burning. As shown by [Hastings et al. \(2019\)](#), this would place the single Be stars very close to the cluster turnoff, which seems to disagree with the quoted observations. The only way to obtain single Be stars a factor of 10-30 below the turnoff luminosity in star clusters is that they are born with near-critical rotation. According to [McSwain & Gies \(2005\)](#), the number of such stars appears to be small. We conclude that it appears likely that binary evolution provides a significant, perhaps dominant, contribution to the Be star population in young star clusters, as suggested by [Schootemeijer et al. \(2018\)](#) and [Klement et al. \(2019\)](#).

6. CONCLUDING REMARKS

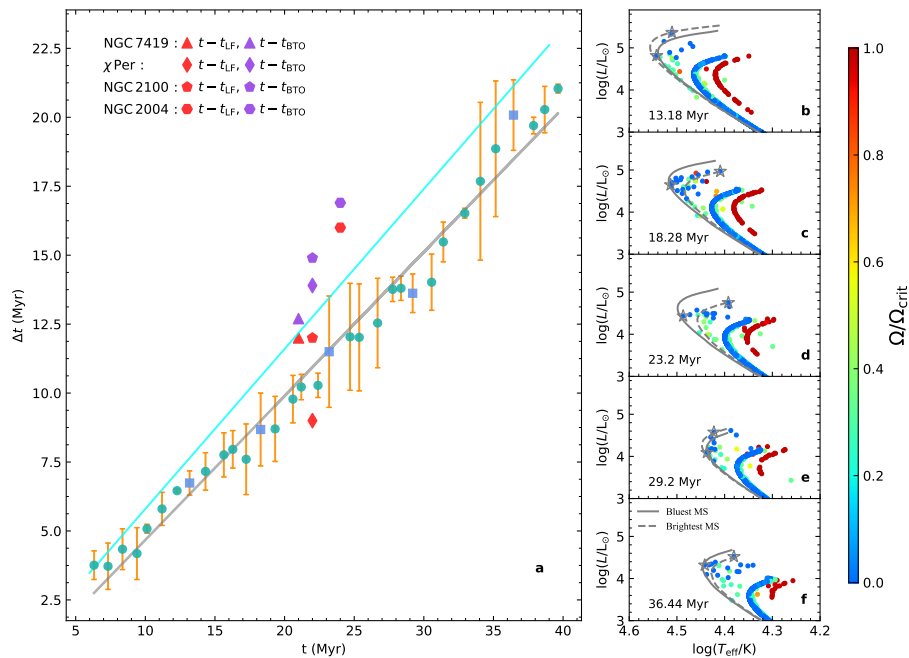


Figure 5. Age spread Δt inferred by the extended MS turnoff from the binary models as a function of cluster age t . To determine the apparent age of the extended turnoff stars in our simulated clusters, we first generate a series of single-star isochrones and then fit these isochrones with two methods, first, using the bluest MS star, and second, using the brightest MS star as to be fitted by the isochrone. Examples are shown in Panels (b) to (f), where the solid gray line describes the best-fitting isochrone for the first, and the dashed gray line describes the best-fitting isochrone for the second method. The model stars used for these fits are indicated by grey star symbols. In Panel (a) we show average of the result from the two methods for 33 different times as green symbols, where the examples from Panels (b) to (f) are marked by blue squares. The error bars represent the difference in the results from the two methods. The gray straight line represents a linear fit to the data as $\Delta t = 0.518t - 0.510$. We also show the results for two Galactic and two LMC clusters of [Beasor et al. \(2019\)](#). Here, we took the age derived from the lowest luminosity red supergiant as the true cluster age ([Beasor et al. 2019](#); [Britavskiy et al. 2019](#)), and show the age discrepancy with the ages derived from the stellar luminosity function (red) and the brightest turnoff star (purple). We display our analytic estimate (Eq. A1) with a cyan line.

Our binary-evolution models produce several distinct morphological features of the MSs of star clusters younger than about 40 Myr. Given that our results emerge from generic binary-evolution model calculations, without applying any fine-tuning, it is striking that they quantitatively reproduce several of the main characteristics of observed MSs of open star clusters. This refers in particular to the extended turnoff region and the corresponding apparent age spread, as well as to the luminosity range of the Be stars in young clusters. Both effects are comprehensively demonstrated by our animation (Fig. 3).

This does not preclude the possibility that other factors are also important. As discussed above, the role of rapidly rotating single stars depends critically on the initial distribution of rotation rates. Also, non-coevality or differences in the initial chemical composition of the cluster stars may be important in some clusters. Our results imply that binary evolution is likely to play a major role in shaping the MSs of star clusters, as long as a substantial fraction of the stars are born in binary systems. A detailed population synthesis study including all of the above factors will help us to confirm this picture, and will have strong implications for our understanding of star and binary formation and evolution, including the origin of the mass ratio and orbital period distribution of close binaries, and the IMF of stars.

ACKNOWLEDGMENTS

C.W. is thankful for the financial support from the CSC scholarship. P.M. acknowledges support from NSF grant AST-1517753 and the Senior Fellow of the Canadian Institute for Advanced Research (CIFAR) program in Gravity and Extreme Universe, both granted to Vassiliki Kalogera at Northwestern University.

APPENDIX

A. APPENDIX: QUANTITATIVE CHARACTERIZATION OF THE MAIN-SEQUENCE FEATURES

We quantify the features of the TBF, RBF, and BBF described in Fig. 1 in Appendix A.1, A.2, and A.3, respectively.

A.1. TBF (*Turnoff binary-evolution feature*)

The apparent age spread indicated by the extended turnoff region is about half of the true age of the simulated stars (see Figure 2 of Niederhofer et al. 2015). This compares well with simple estimates of the binary rejuvenation due to mass accretion and stellar mergers. For a mass-luminosity relation as $L \propto M^\alpha$, and a hydrogen burning lifetime of a star of mass M as $\tau \propto M/L$, the lifetime ratio of two stars is $\tau_1/\tau_2 = (M_1/M_2)^{1-\alpha}$, while their luminosity ratio is $L_1/L_2 = (\tau_1/\tau_2)^{\alpha/(1-\alpha)}$. The maximum possible stellar mass in a cluster with a single-star turnoff mass of $8 M_\odot$ (corresponding to M_1 in the equations above), will be about $14.4 M_\odot$ ($= M_2$), i.e., the result a merger of two $8 M_\odot$ stars (90% of $16 M_\odot$). Therefore, we obtain an equation for the apparent age spread $\tau_1 - \tau_2$ in our cluster with an age τ_1 that is linear in τ_1 , as

$$\tau_1 - \tau_2 = \left[1 - \left(\frac{M_1}{M_2} \right)^{\alpha-1} \right] \tau_1, \quad (\text{A1})$$

and for $M_1/M_2 = 8/14.4$ and for $\alpha = 2.5$, which holds approximately for stars of $14 M_\odot$ and is only a weak function of the mass (see Figure 17 of Köhler et al. 2015), we obtain $\tau_1 - \tau_2 = 0.58\tau_1$.

A.2. RBF (*Red binary-evolution feature*)

We note that our MESA models may underestimate the effect of the centrifugal force on the outermost parts of the stellar models for a rotation faster than about 90% of critical rotation (Paxton et al. 2019). Furthermore, they do not account for the presence of a decretion disk, which may make the star appear redder than predicted here (Rivinius et al. 2013). This does induce an uncertainty in the predicted effective temperature, or any magnitude or color computed from it.

The extent of the RBF in luminosity is determined by the minimum mass ratio for stable mass transfer. For example, at a turnoff masses of $20 M_\odot$ (corresponding to $t \simeq 10$ Myr), the minimum initial mass ratio $q_{\text{min,B}}$ for which a merger during the Case B mass transfer is avoided is $q_{\text{min,B}} \simeq 0.3$, i.e., the minimum stellar mass on the RBF is about $6 M_\odot$ (as little mass is accreted). Just from the mass difference, using the mass-luminosity relation of the form $L \propto M^\alpha$ with $\alpha \simeq 2.5$ (Köhler et al. 2015) implies a luminosity ratio between the brightest and the dimmest RBF star of 20 (1.31 dex). However, due to the large mass difference, while the brightest RBF star is about to finish core hydrogen burning, the dimmest ones are essentially unevolved. We therefore need to consider the difference in the average mean molecular weight μ of the stars, which contributes to the luminosity difference as $L \propto \mu^\beta$. An initial mean molecular weight of $\mu_{\text{SMC}} = 0.59$, the mean molecular weight of helium as $\mu_{\text{He}} = 4/3$, and an average convective core mass fraction of $q_{\text{core}} = 0.25$, yield an average mean molecular weight of our brightest RBF star of $\bar{\mu} = 0.69$, which, with $\beta \simeq 4.5$ (see Figure 17 of Köhler et al. 2015), yields another factor of 2.02 (0.31 dex) for the luminosity ratio, resulting in a total of 41 (1.61 dex), i.e., in more general terms, the luminosity ratio between the brightest and the dimmest RBF star is

$$\frac{L_{\text{top}}}{L_{\text{bottom}}} = \left(\frac{\mu_{\text{He}}}{\mu_{\text{SMC}}q_{\text{core}} + \mu_{\text{He}}(1 - q_{\text{core}})} \right)^\beta \left(\frac{1}{q_{\text{min,B}}} \right)^\alpha. \quad (\text{A2})$$

Considering the dependence of $q_{\text{min,B}}$ on cluster age, i.e., for $t \lesssim 15$ Myr we have $q_{\text{min,B}} \lesssim 0.3$, which rises to $q_{\text{min,B}} \lesssim 0.6$ at 20 Myr and 0.7 at 30 Myr and beyond, the above equation leads to a good characterization of the RBF for the different times shown in Fig. 1.

Due to mass accretion during Case B, the fraction of RBF stars near the turnoff region will be naturally close to one, as observed in many young clusters. At lower luminosities, the RBF star fraction will be proportional to the fraction of Case B binaries that avoid merging.

The temperature separation between RBF and SSI cannot be predicted well by our models. The reason is that the RBF stars rotate at more than 0.98% of critical rotation. The outer layers of current rotating 1D models are not well described for models beyond 0.90% of critical rotation (Paxton et al. 2019).

A.3. BBF (*Blue binary-evolution feature*)

The BBF merges with extended turnoff stars at the highest luminosities. The minimum luminosity is determined in our models by the minimum initial mass ratio for which Case A contact evolution is avoided for at least a fraction of core hydrogen burning, which is $q_{\min,A} = 0.7$ for an initial donor mass of $M_{1,i} = 10 M_{\odot}$, and $q_{\min,A} = 0.35$ for an initial donor mass of $M_{1,i} = 20 M_{\odot}$. We note that our predictions for the evolution of contact systems must be considered as very uncertain, as our models do not allow for heat flows between the two components. Therefore, the more realistic values of $q_{\min,A}$, as well as the number of blue MS stars, may differ significantly from those obtained in our calculation.

REFERENCES

- Ahumada, J. A., & Lapasset, E. 2007, *A&A*, 463, 789, doi: [10.1051/0004-6361:20054590](https://doi.org/10.1051/0004-6361:20054590)
- Atkinson, R. D. E., & Houtermans, F. G. 1929, *Zeitschrift fur Physik*, 54, 656, doi: [10.1007/BF01341595](https://doi.org/10.1007/BF01341595)
- Beasor, E. R., Davies, B., Smith, N., & Bastian, N. 2019, *MNRAS*, 486, 266, doi: [10.1093/mnras/stz732](https://doi.org/10.1093/mnras/stz732)
- Bodensteiner, J., Sana, H., Mahy, L., et al. 2019, The young massive SMC cluster NGC 330 seen by MUSE. I. Observations and stellar content. <https://arxiv.org/abs/1911.03477>
- Britavskiy, N., Lennon, D. J., Patrick, L. R., et al. 2019, *A&A*, 624, A128, doi: [10.1051/0004-6361/201834564](https://doi.org/10.1051/0004-6361/201834564)
- Brott, I., de Mink, S. E., Cantiello, M., et al. 2011, *A&A*, 530, A115, doi: [10.1051/0004-6361/201016113](https://doi.org/10.1051/0004-6361/201016113)
- Cantiello, M., & Langer, N. 2010, *A&A*, 521, A9, doi: [10.1051/0004-6361/201014305](https://doi.org/10.1051/0004-6361/201014305)
- Chaboyer, B., & Zahn, J.-P. 1992, *A&A*, 253, 173
- D’Antona, F., Milone, A. P., Tailo, M., et al. 2017, *Nature Astronomy*, 1, 0186, doi: [10.1038/s41550-017-0186](https://doi.org/10.1038/s41550-017-0186)
- de Mink, S. E., Langer, N., Izzard, R. G., Sana, H., & de Koter, A. 2013, *ApJ*, 764, 166, doi: [10.1088/0004-637X/764/2/166](https://doi.org/10.1088/0004-637X/764/2/166)
- de Mink, S. E., Sana, H., Langer, N., Izzard, R. G., & Schneider, F. R. N. 2014, *ApJ*, 782, 7, doi: [10.1088/0004-637X/782/1/7](https://doi.org/10.1088/0004-637X/782/1/7)
- Detmers, R. G., Langer, N., Podsiadlowski, P., & Izzard, R. G. 2008, *A&A*, 484, 831, doi: [10.1051/0004-6361:200809371](https://doi.org/10.1051/0004-6361:200809371)
- Dufton, P. L., Langer, N., Dunstall, P. R., et al. 2013, *A&A*, 550, A109, doi: [10.1051/0004-6361/201220273](https://doi.org/10.1051/0004-6361/201220273)
- Ekström, S., Meynet, G., Maeder, A., & Barblan, F. 2008, *A&A*, 478, 467, doi: [10.1051/0004-6361:20078095](https://doi.org/10.1051/0004-6361:20078095)
- Georgy, C., Ekström, S., Eggenberger, P., et al. 2013, *A&A*, 558, A103, doi: [10.1051/0004-6361/201322178](https://doi.org/10.1051/0004-6361/201322178)
- Hastings, B., Wang, C., & Langer, N. 2019, arXiv e-prints, arXiv:1912.05290. <https://arxiv.org/abs/1912.05290>
- Heger, A., Langer, N., & Woosley, S. E. 2000, *ApJ*, 528, 368, doi: [10.1086/308158](https://doi.org/10.1086/308158)
- Heger, A., Woosley, S. E., & Spruit, H. C. 2005, *ApJ*, 626, 350, doi: [10.1086/429868](https://doi.org/10.1086/429868)
- Howarth, I. D., Dufton, P. L., Dunstall, P. R., et al. 2015, *A&A*, 582, A73, doi: [10.1051/0004-6361/201526408](https://doi.org/10.1051/0004-6361/201526408)
- Klement, R., Carciofi, A. C., Rivinius, T., et al. 2019, *ApJ*, 885, 147, doi: [10.3847/1538-4357/ab48e7](https://doi.org/10.3847/1538-4357/ab48e7)
- Köhler, K., Langer, N., de Koter, A., et al. 2015, *A&A*, 573, A71, doi: [10.1051/0004-6361/201424356](https://doi.org/10.1051/0004-6361/201424356)
- Langer, N. 1998, *A&A*, 329, 551
- . 2012, *ARA&A*, 50, 107, doi: [10.1146/annurev-astro-081811-125534](https://doi.org/10.1146/annurev-astro-081811-125534)
- Langer, N., Fricke, K. J., & Sugimoto, D. 1983, *A&A*, 126, 207
- Li, C., Sun, W., de Grijs, R., et al. 2019, *ApJ*, 876, 65, doi: [10.3847/1538-4357/ab15d2](https://doi.org/10.3847/1538-4357/ab15d2)
- Maeder, A. 1987, *A&A*, 178, 159
- Mahy, L., Sana, H., Abdul-Masih, M., et al. 2019, arXiv e-prints, arXiv:1912.08107. <https://arxiv.org/abs/1912.08107>
- Marchant, P., Langer, N., Podsiadlowski, P., et al. 2017, *A&A*, 604, A55, doi: [10.1051/0004-6361/201630188](https://doi.org/10.1051/0004-6361/201630188)
- Marchant, P., Langer, N., Podsiadlowski, P., Tauris, T. M., & Moriya, T. J. 2016, *A&A*, 588, A50, doi: [10.1051/0004-6361/201628133](https://doi.org/10.1051/0004-6361/201628133)
- McSwain, M. V., & Gies, D. R. 2005, *ApJS*, 161, 118, doi: [10.1086/432757](https://doi.org/10.1086/432757)

- Milone, A. P., Marino, A. F., Di Criscienzo, M., et al. 2018, *MNRAS*, 477, 2640, doi: [10.1093/mnras/sty661](https://doi.org/10.1093/mnras/sty661)
- Niederhofer, F., Georgy, C., Bastian, N., & Ekström, S. 2015, *MNRAS*, 453, 2070, doi: [10.1093/mnras/stv1791](https://doi.org/10.1093/mnras/stv1791)
- Packet, W. 1981, *A&A*, 102, 17
- Paxton, B., Bildsten, L., Dotter, A., et al. 2011, *ApJS*, 192, 3, doi: [10.1088/0067-0049/192/1/3](https://doi.org/10.1088/0067-0049/192/1/3)
- Paxton, B., Cantiello, M., Arras, P., et al. 2013, *ApJS*, 208, 4, doi: [10.1088/0067-0049/208/1/4](https://doi.org/10.1088/0067-0049/208/1/4)
- Paxton, B., Marchant, P., Schwab, J., et al. 2015, *ApJS*, 220, 15, doi: [10.1088/0067-0049/220/1/15](https://doi.org/10.1088/0067-0049/220/1/15)
- Paxton, B., Smolec, R., Schwab, J., et al. 2019, *ApJS*, 243, 10, doi: [10.3847/1538-4365/ab2241](https://doi.org/10.3847/1538-4365/ab2241)
- Petrovic, J., Langer, N., & van der Hucht, K. A. 2005, *A&A*, 435, 1013, doi: [10.1051/0004-6361:20042368](https://doi.org/10.1051/0004-6361:20042368)
- Pols, O. R., Cote, J., Waters, L. B. F. M., & Heise, J. 1991, *A&A*, 241, 419
- Ramírez-Agudelo, O. H., Sana, H., de Mink, S. E., et al. 2015, *A&A*, 580, A92, doi: [10.1051/0004-6361/201425424](https://doi.org/10.1051/0004-6361/201425424)
- Rivinius, T., Carciofi, A. C., & Martayan, C. 2013, *A&A Rv*, 21, 69, doi: [10.1007/s00159-013-0069-0](https://doi.org/10.1007/s00159-013-0069-0)
- Russell, H. N. 1914, *Popular Astronomy*, 22, 275
- Salpeter, E. E. 1955, *ApJ*, 121, 161, doi: [10.1086/145971](https://doi.org/10.1086/145971)
- Sana, H., de Mink, S. E., de Koter, A., et al. 2012, *Science*, 337, 444, doi: [10.1126/science.1223344](https://doi.org/10.1126/science.1223344)
- Sanyal, D., Grassitelli, L., Langer, N., & Bestenlehner, J. M. 2015, *A&A*, 580, A20, doi: [10.1051/0004-6361/201525945](https://doi.org/10.1051/0004-6361/201525945)
- Sanyal, D., Langer, N., Szécsi, D., -C Yoon, S., & Grassitelli, L. 2017, *A&A*, 597, A71, doi: [10.1051/0004-6361/201629612](https://doi.org/10.1051/0004-6361/201629612)
- Schneider, F. R. N., Izzard, R. G., Langer, N., & de Mink, S. E. 2015, *ApJ*, 805, 20, doi: [10.1088/0004-637X/805/1/20](https://doi.org/10.1088/0004-637X/805/1/20)
- Schneider, F. R. N., Ohlmann, S. T., Podsiadlowski, P., et al. 2019, *Nature*, 574, 211, doi: [10.1038/s41586-019-1621-5](https://doi.org/10.1038/s41586-019-1621-5)
- Schneider, F. R. N., Podsiadlowski, P., Langer, N., Castro, N., & Fossati, L. 2016, *MNRAS*, 457, 2355, doi: [10.1093/mnras/stw148](https://doi.org/10.1093/mnras/stw148)
- Schneider, F. R. N., Izzard, R. G., de Mink, S. E., et al. 2014, *ApJ*, 780, 117, doi: [10.1088/0004-637X/780/2/117](https://doi.org/10.1088/0004-637X/780/2/117)
- Schootemeijer, A., Götberg, Y., de Mink, S. E., Gies, D., & Zapartas, E. 2018, *A&A*, 615, A30, doi: [10.1051/0004-6361/201731194](https://doi.org/10.1051/0004-6361/201731194)
- Spruit, H. C. 2002, *A&A*, 381, 923, doi: [10.1051/0004-6361:20011465](https://doi.org/10.1051/0004-6361:20011465)
- van Bever, J., & Vanbeveren, D. 1998, *A&A*, 334, 21
- Wang, L., Gies, D. R., & Peters, G. J. 2018, *ApJ*, 853, 156, doi: [10.3847/1538-4357/aaa4b8](https://doi.org/10.3847/1538-4357/aaa4b8)
- Yang, W., Meng, X., Bi, S., et al. 2011, *ApJL*, 731, L37, doi: [10.1088/2041-8205/731/2/L37](https://doi.org/10.1088/2041-8205/731/2/L37)